Journal of Magnetism and Magnetic Materials ∎ (∎∎∎∎) ∎∎∎–∎∎∎

Contents lists available at ScienceDirect

Journal of Magnetism and Magnetic Materials

journal homepage: www.elsevier.com/locate/jmmm

Hysteresis modelling of GO laminations for arbitrary in-plane directions taking into account the dynamics of orthogonal domain walls

A.P.S. Baghel [a,*], B. Sai Ram [a], K. Chwastek [b], L. Daniel [c], S.V. Kulkarni [a]

[a] Department of Electrical Engineering, Indian Institute of Technology Bombay, Mumbai 400076, India
[b] Department of Electrical Engineering Czestochowa University of Technology, Poland
[c] Group of Electrical Engineering-Paris (GeePs), CNRS(UMR8507)/CentraleSupelec/UPMC/Univ Paris-Sud, 11 rue Joliot-Curie, 91192 Gif-sur-Yvette, France

ARTICLE INFO

Article history:
Received 12 November 2015
Received in revised form
31 January 2016
Accepted 4 February 2016

Keywords:
Hysteresis loops
Grain-oriented laminations
Anisotropy
Domain walls
Jiles-Atherton model

ABSTRACT

The anisotropy of magnetic properties in grain-oriented steels is related to their microstructure. It results from the anisotropy of the single crystal properties combined to crystallographic texture. The magnetization process along arbitrary directions can be explained using phase equilibrium for domain patterns, which can be described using Neel's phase theory. According to the theory the fractions of 180° and 90° domain walls depend on the direction of magnetization. This paper presents an approach to model hysteresis loops of grain-oriented steels along arbitrary in-plane directions. The considered description is based on a modification of the Jiles–Atherton model. It includes a modified expression for the anhysteretic magnetization which takes into account contributions of two types of domain walls. The computed hysteresis curves for different directions are in good agreement with experimental results.

1. Introduction

The magnetic properties of grain-oriented steels (hysteresis loops, losses, permeability, etc) exhibit substantial anisotropy due to the strong anisotropy of Iron–Silicon crystals combined to a very pronounced crystallographic texture [1,2]. From a practical point of view, the development of physics-based descriptions of magnetization processes, taking into account anisotropy effects, is crucial for proper material characterization. Grain-oriented (GO) Iron–Silicon steels are widely used in electromagnetic devices such as power transformers and large rotating machines [3–6]. Standard characterization techniques are most often applied along the two principal directions, namely the rolling direction (RD) and the transverse one (TD) [7–9]. However, in many applications (e.g. core joints and corners in transformers) the magnetization process happens along directions different from the aforementioned two ones [10,11]. It is thus important to develop appropriate tools for material behavior description in these conditions.

Among numerous hysteresis models three of them have gained much attention of scientists and engineers [12]. These are Preisach–Mayergoyz, Stoner–Wohlfarth and Jiles–Atherton models. The Preisach model is based on the concept that hysteresis loop can be described from the superposition of contributions from elementary entities called hysterons [13,14]. This description has been studied in detail since its inception in 1935 and substantially improved by I. D. Mayergoyz [14]. A thorough discussion of individual modifications of the Preisach model is beyond the scope of the present paper and the readers are referred to the monograph [14]. For the subject of the present paper, it suffices to focus on the vector extension of the Preisach model [15]. It considers individual distributions of hysterons for different magnetization directions. Hence, the vector model is constructed as a superposition of several scalar Preisach models. The idea has been verified and further extended for instance to consider possible couplings between distributions of individual axes [16,17], to extend the problem to 3D models [18], to deal with efficient numerical implementation [19,20], or to describe the phenomena of accommodation and aftereffect [21].

The Stoner–Wohlfarth description is derived from micromagnetics and naturally introduces the anisotropy of individual grain as a key parameter [22]. It is inherently vectorial in nature and it has been extensively used by scientists working on thin films. In practice it is very often combined with the Preisach model [15,23]. Other approaches-so called multiscale approaches -have also been proposed to deduce the macroscopic behavior of magnetic materials from energetic considerations at the magnetic domain scale [24–26].

The third popular hysteresis model is the Jiles–Atherton approach [27]. It introduces a limited number of parameters to

* Corresponding author.

http://dx.doi.org/10.1016/j.jmmm.2016.02.007
0304-8853/

define the anhysteretic magnetization and the hysteresis contribution. It is given in the form of a set of algebraic equations and an ordinary differential equation, which can be implemented in numerical codes. It provides a macroscopic material response to a given loading. The original model has been further extended for instance to consider vectorial loadings [28–30], or to introduce advanced description of the anhysteretic curve [31,32]. A recent modification in the JA model is proposed for describing hysteresis loops of grain-oriented steels along the two principal directions [33]. In previous works the usefulness of the model was assessed for the characterization of hysteresis loops, including minor loops, for two principal directions either in quasi-static or dynamic conditions [34,35].

The magnetization process can be described in terms of complex variations of the domain pattern with directions of the applied field [3–4]. A theoretical study of the angular dependence of magnetic properties in GO materials is reported in [4] using the domain phase theory. An experimental study, reported in Ref. [3], supports the theory with observation of different proportions of 180° and 90° domain walls (DWs) in different directions. Magnetic properties along RD can be modeled using the contribution of 180° DWs only, whereas, in other directions, these can be explained in terms of 180° and 90° DWs [4]. Anisotropy in the magnetic behavior of GO materials is evident in Fig. 1 showing measured quasi-static hysteresis loops (details of measurement procedure is given in Section-IV) at angles 0°, 45° and 90° from the rolling direction.

Hysteresis loops along different directions can be described from the complicated interplay between two magnetization mechanisms viz., the irreversible motion of domain walls and the irreversible rotation of domain magnetization vectors [36]. Lower initial values of permeability and higher coercivity values along TD can be attributed to an initial domain configuration mainly oriented towards RD so that the magnetization process involves a significant amount of magnetization rotation [7,37]. When a field is applied along TD, the magnetization process is completed first by nucleation and growth of domains perpendicular to RD, and then rotation to align them with TD [7]. Therefore, a hysteresis model must have the ability to consider these mechanisms (wall translation and magnetization rotation) and to relate the internal parameters to corresponding microstructure. Such a model will allow considering the case of rotating flux in electromagnetic applications. When integrated into system design CAD tools, it will allow an accurate computation of fields in electromagnetic devices.

This paper presents the modeling of hysteresis loops in arbitrary in-plane directions for a sheet of grain-oriented steel on the account of contributions of 180° and 90° DWs motions and the magnetization rotation in the magnetization process. The model adapts the assumptions from the Neel's phase theory [38]. It computes the anhysteretic magnetization using a relationship that includes energy contributions from both types of walls using two orthogonal components of the applied field along RD and TD. Hysteretic effects are included in the model using the pinning concept of the JA approach. An additional parameter, which represents the volume fractions of the two types of DWs in the material, is used in the model. The proposed model is validated using measured hysteresis loops along different directions. Computed and experimental results are in close agreement.

2. Domains and magnetization processes

As a first approximation GO Fe–Si materials can be considered as single crystals because the axes of individual crystallites are aligned with the global cubic axes [39]. In single crystals, prior

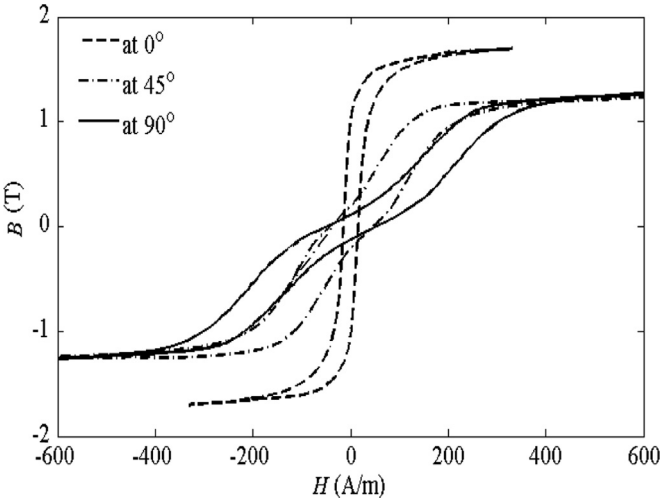

Fig. 1. Measured quasi-static hysteresis loops for a GO material at different angles (0°, 45°, and 90°).

knowledge of the space orientation of easy magnetization axes can be used to define domain structures/patterns [3–4,40]. The domain structure of a material sample can be described in terms of the coexistence of phases provided that the external field is large enough to overcome pinning fields. Typical hysteresis loops of GO materials can be reproduced using various forms of this phase equilibrium [4]. Magnetocrystalline anisotropy plays a major role in the phase equilibrium for these materials [40]. The anisotropy energy for a cube with a positive anisotropic constant (K_1), produces six equivalent energy minima, corresponding to the magnetization vector $\boldsymbol{m}$ pointing along the positive or negative direction of the three orthogonal easy axes. Thus, there are six magnetic phases and a given domain structure represents a particular mixture of these phases [40]. Domains in demagnetized GO laminations are mostly oriented along RD and can be described with two phases ([001] and [$00\bar{1}$]). The domains change in a complex manner when the field is applied along directions other than RD. The domain pattern of a sheet along its plane and cross section in a demagnetized state is shown in Fig. 2, with magnetization m_s directed along [001] and [$00\bar{1}$] (i.e. RD). Hence, in the demagnetized state, the sample has only two phases with magnetization aligned with RD (positive and negative). When an applied field is applied along RD, the domains with favorable orientation will expand at the expense of other domains. In the

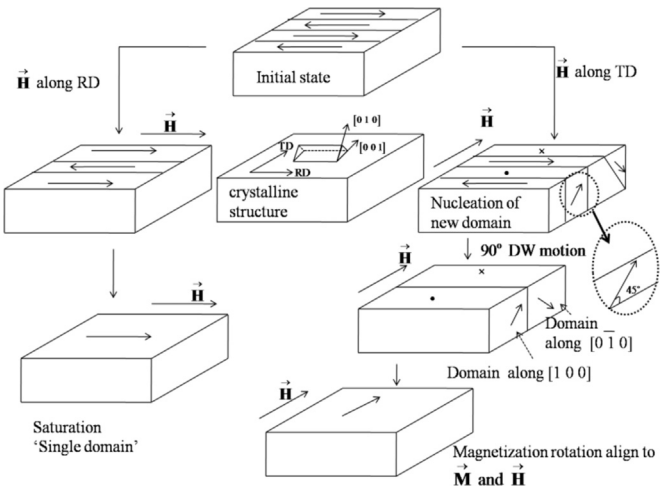

Fig. 2. Domain pattern of a single crystal (110) [001] when field is applied along (a) RD (b) TD [7].

saturation state, the sample can be represented by a single domain structure. Therefore the RD loops of GO laminations can be defined in terms of these two phase evolutions ([001] and [00$\bar{1}$]). On the other hand, when a magnetic field is applied along TD, the domains will change in a more complex fashion. As the applied field increases, the basic 180° domains will get transformed through 90° domain wall processes. The domains in the sheet cross section with the magnetization directed along [100] and [0$\bar{1}$0] are shown in Fig. 2. This domain structure reduces the magnetization component normal to the sheet surface to zero [4,7]. Hence, the sample has a mode (known as mode-I) of four phases in this procedure which terminates at maximum magnetization according to Kaya's rule [4,40]. If the applied field further increases, the two phases coexist in equilibrium and the magnetization further increases by domain magnetization rotation. Therefore, in the magnetization process along TD, the sample will have a mixture of both 180° and 90° DWs and it exhibits a hysteresis loop with a complex shape. The magnetization process and the corresponding domain structures have consequences at the macroscopic level in terms of magnetic induction, coercivity, permeability and losses. The angular dependence of these variables with the texture of materials is discussed in [41]. The value of maximum magnetization (m_s) depends on the domain structure (i.e., the balance between different phases) of the material sample [4]. The value of the maximum (technical saturation) magnetization in different directions for these materials can be calculated according to Kaya's rule [4,40]. This "maximum" magnetization is also referred to as "*apparent saturation magnetization*" and its directional dependence can be explained by demagnetising effects due to the complex domain structure. It is important here to note that the "*final*" or "*true*" *saturation magnetization* is the same for any direction and it is markedly higher than the "*technical*" *or* "*apparent*" *saturation magnetization*" [40]. An attempt to explain the anisotropy in the coercive field and losses using subdivision of hysteresis loss into low induction and high induction loss components is made in Ref. [42].

3. Hysteresis model

For an ideal Goss-textured material, the (110) plane is parallel to the surface of the sheet and the [001] direction lies along RD [43]. The magnetic field in GO laminations is generally analyzed in two dimensions because of their small thickness. A modified JA hysteresis model to describe hysteresis loops along RD and TD of GO steels has been proposed in [33]. The model uses a single lamination model as shown in Fig. 3. Two magnetic moments m_1 and m_2 in the plane of the lamination, need to rotate from 0° to 180° due to symmetry in the anisotropy energy [44]. The energy equation, in presence of anisotropy, is [44]:

$$E = -\mu_0 m_s \cdot (H + \alpha M) + E_{an}. \tag{1}$$

According to Ref. [45], the anisotropy energy expression can be written as

$$E_{an} = K_0 + K_1\left(\cos^2\varphi \cdot \sin^2\varphi + \frac{\sin^4\varphi}{4}\right) + K_2\frac{\cos^2\varphi \cdot \sin^4\varphi}{4} \tag{2}$$

where φ is the angle between the magnetization direction and RD. The anisotropy constants K_0 and K_2 can be neglected without a significant loss of accuracy [45].

The model, reported in Ref. [33], includes the magnetocrystalline anisotropic energy on the account of modified anhysteretic magnetization. Since the two basic types of domain walls are responsible for the magnetization process in these materials, the model can accurately predict hysteresis loops along the two

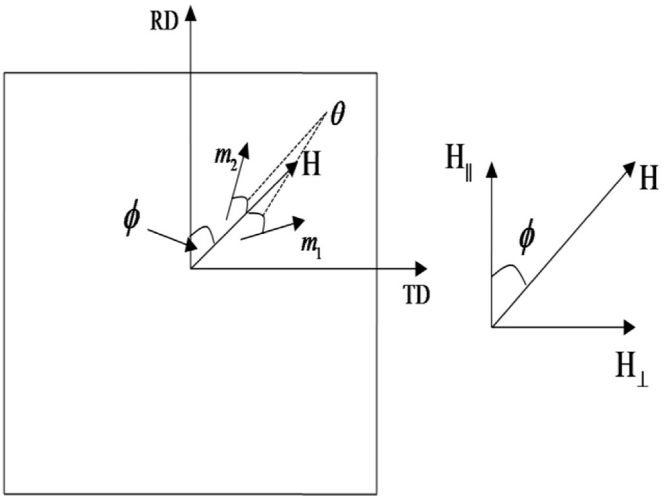

Fig. 3. A single sheet model and field components.

principal directions. In other directions, magnetization process can be described by introducing the proportions of these two basic DWs [3].

For an applied field at an arbitrary angle ϕ from RD, the magnetic field can be decomposed into two orthogonal components as:

$$H_{\parallel} = H\cos(\phi) \text{and } H_{\perp} = H\sin(\phi) \tag{3}$$

The first term of the energy Eq. (1) can be rewritten as the sum of two energy terms corresponding to the two orthogonal field components as:

$$E_s = -\left[(\mu_0 m_s \cdot (H_{\parallel} + \alpha M_{\parallel})) + (\mu_0 m_s \cdot (H_{\perp} + \alpha M_{\perp})\right) \tag{4}$$

The equation is consistent with the basic model given in [33] because when the field is along RD, only the first term will contribute to the total energy and when the field is along TD only the second term will be non-zero. Now, the total anisotropy energy can also be rewritten as the sum of two energy terms corresponding to these two field components. The anisotropic energies of the two magnetic moments m_1 and m_2 can be expressed as [33]:

$$E_{an}(1) = K_{an}\left[r_x\left(\cos^2\varphi_{11}\cdot\sin^2\varphi_{11} + \frac{\sin^4\varphi_{11}}{4}\right) + (1 - r_x)\left(\cos^2\varphi_{12}\cdot\sin^2\varphi_{12} + \frac{\sin^4\varphi_{12}}{4}\right)\right] \tag{5}$$

$$E_{an}(2) = K_{an}\left[r_x\left(\cos^2\varphi_{21}\cdot\sin^2\varphi_{21} + \frac{\sin^4\varphi_{21}}{4}\right) + (1 - r_x)\left(\cos^2\varphi_{22}\cdot\sin^2\varphi_{22} + \frac{\sin^4\varphi_{22}}{4}\right)\right] \tag{6}$$

where

$\varphi_{11} = \phi_1 - \theta$; $\varphi_{12} = \phi_2 - \theta$; $\varphi_{21} = \phi_1 + \theta$ and $\varphi_{22} = \phi_2 + \theta$, whereas θ is the angle between the applied field and the magnetic moments. ϕ_1 and ϕ_2 are 0° and 90°, respectively. r_x is the proportion parameter which is related to the volume fractions of the two domain walls.

When a field is applied along RD, the parameter is 1 and when the applied field is along TD, it is zero. For the intermediate directions it will take different values between 0 and 1. Now, the total energy equation becomes:

Please cite this article as: A.P.S. Baghel, et al., Journal of Magnetism and Magnetic Materials (2016), http://dx.doi.org/10.1016/j.jmmm.2016.02.007

$$E = E_s + E_{an}(1) + E_{an}(2) \tag{7}$$

The anhysteretic magnetization can be expressed as a function of the magnetization direction [44]:

$$M_{an} = m_s \frac{\int_0^{\pi} \exp(E/k_B T)\sin\theta\cos\theta\, d\theta}{\int_0^{\pi} \exp(E/k_B T)\sin\theta\, d\theta}. \tag{8}$$

Eq. (8) is consistent with the Langevin function in the case of zero average anisotropy energy ($K_1 = 0$), as per the modification reported in [46]. This equation can be integrated numerically in order to compute the anhysteretic magnetization. The hysteresis curve may be modeled similarly like in the JA approach. An appropriate offset to the anhysteretic magnetization may be introduced in order to take into account the irreversible magnetization processes [27]. The relationship for the differential susceptibility in the JA model is given as,

$$\frac{dM}{dH} = \left[\frac{M_{an}(H) - M_{irr}(H)}{(k\delta/\mu_0) - \alpha(M_{an}(H) - M_{irr}(H))} + c\left(\frac{dM_{an}}{dH} - \frac{dM}{dH}\right)\right] \tag{9}$$

where M is the total magnetization, H is the applied magnetic field, M_{an} is the anhysteretic magnetization, M_{irr} is the irreversible magnetization, μ_0 is the magnetic permeability of vacuum, and δ is the directional parameter taking the values: $+1$ for $dH/dt > 0$ and -1 for $dH/dt < 0$.

The extended model contains seven parameters, including an additionally introduced parameter (r_x). Their values have to be determined using an estimation procedure, for example with a direct iterative method [47], a heuristic [48] or a hybrid technique [49]. It is important to remark that the inverse form of the model may be written analytically. This form may be easily implemented into finite element analysis tools. Moreover it is useful in order to compare the modeling results with measurements carried out under standard conditions, as described in the IEC 60404 Standard (Epstein frame and Single Sheet Tester) in which time dependence of induction B is controlled. The inverse from can be obtained from relationship (9) as [43]:

$$\frac{dM}{dB} = \left[\frac{\left(\frac{c}{\mu_0}\frac{dM_{an}}{dH_e}\right) + \left((1-c)\frac{dM_{irr}}{dB_e}\right)}{1 + \left((1-\alpha)c\frac{dM_{an}}{dH_e}\right) + \left(\mu_0(1-\alpha)(1-c)\frac{dM_{an}}{dH_e}\right)}\right]. \tag{10}$$

4. Modeling of hysteresis loops in arbitrary directions

Measurements are carried out using a standard single sheet tester (SST) (Model: MGP 200 D). Material samples are cut at angles of 0°, 10°, 20°, 30°,..., 90° with respect to RD of a highly grain-oriented (HGO, grade:27-MOH) material. The thickness of the samples is 0.27 mm, the length is 200 mm, and the width is 29.5 mm. The measurement frequency is set to 1 Hz. It is assumed that the effects of eddy currents on the hysteresis loops can be neglected at this frequency [50].

First, the extended model is applied to quasi-static hysteresis loops along the principal directions. The model parameters for the measured RD and TD curves are obtained using the hybrid technique reported in [49]. The optimization procedure is repeated 15 times in order to ensure repetitiveness of the results. The best-fit values for model parameters are given in Table 1.

Table 1
Optimized Parameters for RD and TD.

Angle	m_s (A/m)	a (A/m)	k (A/m)	α	c	K_1(J/m^3)	r_x
$\theta=0°$	1.425×10^6	30	20	5.1×10^{-5}	0.33	1.4×10^2	1
$\theta=90°$	1.11×10^6	33	29	5.1×10^{-5}	0.33	1.7×10^2	0

For the rolling direction loops, only 180° DWs (two phases) will be present in the sample. For the transverse direction the domains are arranged in a rather complex manner, as 90° domain walls are also present. The measured and computed RD and TD curves are shown in Fig. 4. Maximum values of mean squared error do not exceed 6.7% (the highest error is obtained at the knee region on the transverse direction loop).

Next the model is applied to hysteresis loops along other directions. As discussed in the previous section, a sequence of different phases appears in the magnetization process, with a mixture of both 180° and 90° DWs. When the field is applied at any angle with respect to RD, the domain patterns (in the presence of 90° DWs) lead to a sequence of different modes [4]. Some of the model parameters are chosen to vary with the direction of the applied field. Since the maximum value of the magnetization due to domain wall motion varies with direction according to Kaya's rule [4], the model parameter representing saturation magnetization, m_s, depends on the direction of the applied field. The model parameters a (form factor) and k (pinning factor) depend on the domain structure of the materials [51]. Therefore, these parameters are also kept free to vary with respect to the direction of the applied field. The model parameter K_1 is used to adjust the insufficient description of the material anisotropy and particularly of the role of the initial domain configuration in the magnetization process. Hence it is made to depend on the magnetization angle. The proportion parameter (r_x) will also vary to take into account different proportions of the two types of DWs in different directions. The two remaining parameters of the model, α (mean field parameter) and c (domain wall bowing parameter), can be assumed to be independent of the direction of the applied field and remain the same for different magnetic phases [52]. Hence, five model parameters (m_s, a, k, K_1, and r_x) have to be estimated, whereas α and c are kept fixed. The optimized parameters for hysteresis loops at different angles are given in Table 2. The magnetization process is basically due to movements of tilted 180° DWs for a magnetic field orientation up to $\theta \approx 30°$ as it is confirmed in [1] using the normalized hysteresis loss. At higher θ values, a transition of 90° DWs occurs and a sharp increase in the hysteresis loss due to irreversible rotation of domain magnetization can be observed. It is also confirmed by sharp changes in the values of the parameters (K_1 and r_x) at $\theta \approx 30°$ in the proposed model.

The measured and computed curves at different intermediate angles are shown in Figs. 5–6 for angles (10°, 20°, 30°…..90°) from the rolling direction.

Computed and experimental curves are in reasonably close agreement as evident from the figures. The highest mean squared error value is not more than 8.2% for loops in arbitrary directions (the highest error is for $\theta = 80°$). The angular variations of the two model parameters k and a, which strongly depend on the domain structure of the material, are shown in Fig. 7.

The trends obtained for these parameters can also be compared with Orientation Distribution Functions (ODF)-based description recently examined in [53]. This is particularly so for the k parameter, as it is interpreted as the product of the pinning site density and their average energy [27]. Assuming as a first approximation, that this parameter is approximately equal to coercivity, which controls power losses, it follows that the angular dependence of parameter (k) should be somewhat similar to that described by the Lankford parameter in [53]. The trend is indeed followed quite neatly up to 50–60°. However there are some discrepancies above 60°. The discrepancy between the values obtained from the estimation procedure and evaluated from the ODF theory did not exceed 15% up to 60°. This may indicate that for higher angles the

Please cite this article as: A.P.S. Baghel, et al., Journal of Magnetism and Magnetic Materials (2016), http://dx.doi.org/10.1016/j.jmmm.2016.02.007

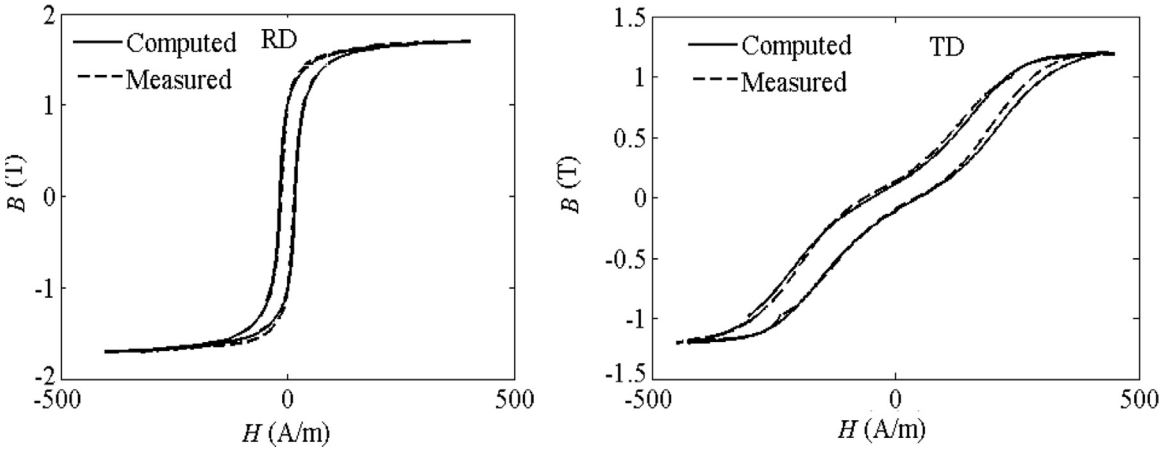

Fig. 4. Measured and computed hysteresis loops (along RD and TD).

Table 2
Optimized Model Parameters at Different Angles.

Angle	m_s (A/m)	a (A/m)	k (A/m)	α	c	K_1(J/m^3)	r_x
$\theta=10°$	1.30×10^6	32	25	5.1×10^{-5}	0.33	1.5×10^2	0.92
$\theta=20°$	1.20×10^6	42	35	5.1×10^{-5}	0.33	1.7×10^2	0.85
$\theta=30°$	1.02×10^6	43	38	5.1×10^{-5}	0.33	1.4×10^3	0.48
$\theta=40°$	1.01×10^6	54	47	5.1×10^{-5}	0.33	1.8×10^3	0.46
$\theta=50°$	9.5×10^5	56	49	5.1×10^{-5}	0.33	1.9×10^3	0.45
$\theta=60°$	9.9×10^5	57	50	5.1×10^{-5}	0.33	2.2×10^3	0.43
$\theta=70°$	9.92×10^5	58	53	5.1×10^{-5}	0.33	1.93×10^3	0.42
$\theta=80°$	1.05×10^6	60	56	5.1×10^{-5}	0.33	1.91×10^3	0.40

roles of 180° and 90° DWs are to some extent interchanged which could indicate another dominant dissipation mechanism, different from the domain wall motion.

5. Conclusions

Grain-oriented laminations show direction-dependent magnetic properties due to their strong crystallographic structure. The macroscopic properties can be described in terms of 180° and 90° domain wall movements and associated phase equilibrium. Bases on the Jiles–Atherton model, this paper presents an approach to model hysteresis loops along arbitrary directions using the domain phase theory to describe average magnetic domain structures. The modeling along arbitrary directions is achieved by considering separately the contributions of 180° and 90° domain walls. A new proportion parameter (r_x) is defined in the model to take into account different volume fractions of the two basic types of DWs. The model has the ability to approximate hysteresis loops for any magnetization angle from RD to TD in GO laminations. The measured and computed curves at different angles are in close

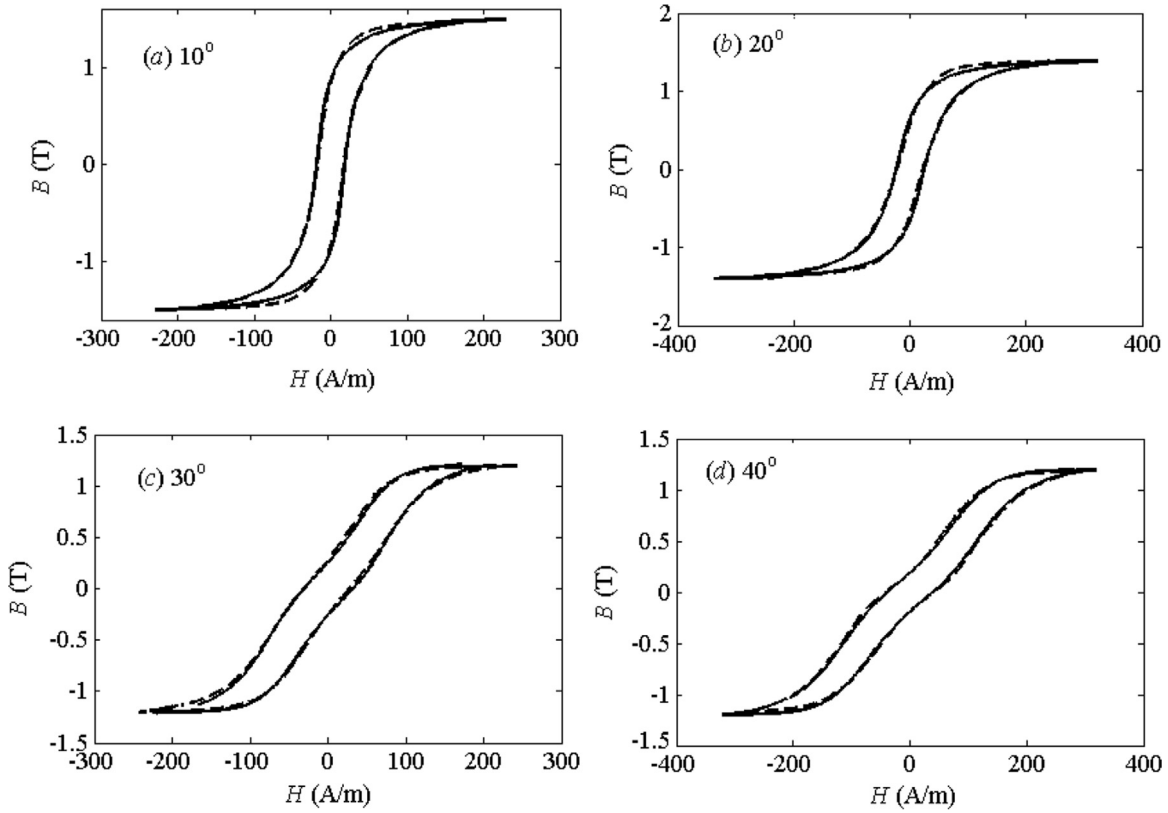

Fig. 5. Measured (dashed line) and computed (solid line) hysteresis loops at different angles (10°, 20°, 30°, and 40°).

Please cite this article as: A.P.S. Baghel, et al., Journal of Magnetism and Magnetic Materials (2016), http://dx.doi.org/10.1016/j.jmmm.2016.02.007

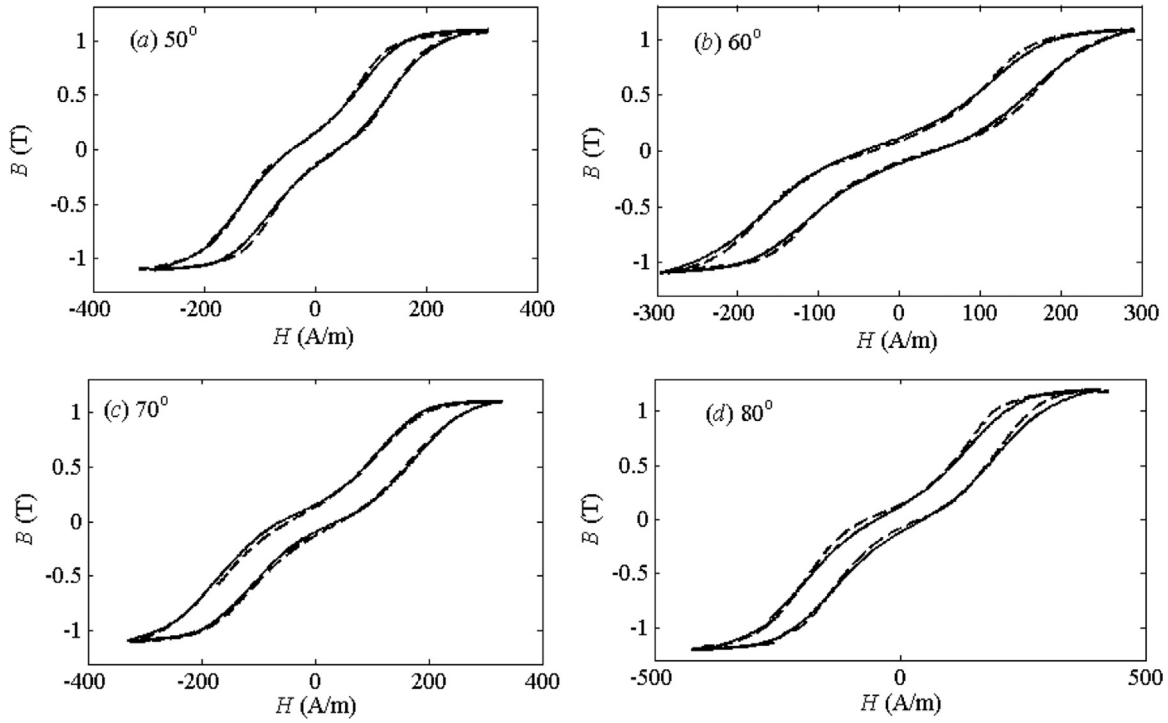

Fig. 6. Measured (dashed line) and computed (solid line) hysteresis loops at different angles (50°, 60°, 70°, and 80°).

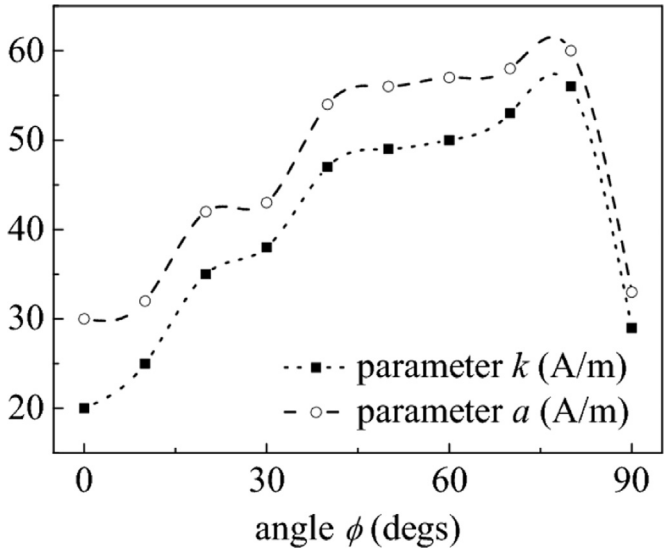

Fig. 7. Angular variations of the model parameters (k and a).

agreement. The model can be useful for the analysis of rotational hysteresis losses in many applications where the flux is not aligned with the principal directions, for example, at T-joints of power transformers and teeth regions of large rotating machines.

The proposed approach could be further extended to consider the effect of mechanical stress. It could shed some light on the physics of coupled magneto-mechanical effects after slight modifications, and notably it may lead to an appropriate extension in the definition of the effective field. In the case of magneto-mechanical loadings, the two types of domain walls are active whichever is the magnetization direction as pointed out in [54–55]. A more complex description of the domain microstructure and its evolution is then required as shown in [56]. The development of a coupled anisotropic extension of the JA model is a potential direction for further study in this research area.

Acknowledgments

The authors would like to thank Crompton Greaves Ltd., Mumbai, India, for providing experimental facilities. The authors would also be grateful to Dr. Satish Shekhawat, a PhD graduate from MEMS Dept., IIT Bombay, for his valuable inputs in experimentations.

References

[1] L.R. Dupre, F. Fiorillo, J. Melkebeek, A.M. Rietto, C. Appino, J. Magn. Magn. Mater. 215 – 216 (2000) 112.
[2] V. Paltanea, G. Paltanea, Mater. Sci. Forum 670 (2011) 66.
[3] S. Shin, R. Schaefer, B.C. DeCooman 07A307-1, J. Appl. Phys. 109 (2011).
[4] F. Fiorillo, L.R. Dupre, C. Appino, A.M. Rietto, IEEE Trans. Magn. 38 (2002) 1467.
[5] H. Pfützner, IEEE Trans. Magn. 30 (1994) 2802.
[6] A. Basak, P. Caryotis, IEEE Trans. Magn. 20 (1984) 1560.
[7] O. Hubert, L. Daniel, J. Magn. Magn. Mater 320 (2008) 1412.
[8] F. Fiorillo, Measurement and Characterization of Magnetic Materials, first ed., Elsevier-Academic Press, Amsterdam, 2004.
[9] R. Szewczyk, Application of Jiles-Atherton model for modelling magnetization characteristics of textured electrical steel magnetized in easy or hard axis, in: R. Szewczyk, et al., (Eds.), Progress in Automation, Robotics and Measuring Techniques, Book Series Advances in Intelligent Systems and Computing, 350, Springer-Verlag, Berlin-Heidelberg, 2015, pp. 293–302.
[10] H. Yoon, C.S. Koh, COMPEL 33 (2014) 14.
[11] A. Moses, J. Mater. Eng. Perform 1 (1992) 235.
[12] E. Cardelli, Advances in hysteresis modeling, chapter, in: K.H.J. Buschow (Ed.), Handbook of Magnetic Materials, 24, Science Direct Publication, 2015, pp. 323–409.
[13] F. Preisach, Z. Phys. 94 (1935) 277.
[14] I.D. Mayergoyz, Mathematical Models of Hysteresis and Their Applications, first ed., Elsevier-Academic Press, Amsterdam, 2003.
[15] I.D. Mayergoyz, J. Appl. Phys. 63 (1988) 2995.
[16] A.A. Adly, S.K. Abd-El-Hafiz, IEEE Trans. Magn. 42 (2006) 1518.
[17] A.A. Adly, S.K. Abd-El-Hafiz, Physica B 407 (2012) 1350.
[18] I.D. Mayergoyz, G. Friedman, IEEE Trans. Magn. 24 (1988) 2928.
[19] G. Friedman, D. Ahya, IEEE Trans. Magn. 30 (1994) 4386.

[20] E. Dlala, A. Belahcen, K.A. Fonteyn, M. Belkasim, IEEE Trans. Magn. 46 (2010) 918.
[21] E. Della Torre, IEEE Press, New York 1999.
[22] E.C. Stoner, E.P. Wohlfarth, Philos. Trans. R. Soc. Lond. A240 (1948) 599.
[23] G. Kahler, E. Della Torre, E. Cardelli, IEEE Trans. Magn. 46 (2010) 21.
[24] W.D. Armstrong, J. Appl. Phys. 81 (1997) 232.
[25] H. Hauser, J. Appl. Phys. 96 (5) (2004) 2753.
[26] L. Daniel, M. Rekik, O. Hubert, Arch. Appl. Mech. 84 (9) (2014) 1307.
[27] D.C. Jiles, D.L. Atherton, J. Magn. Magn. Mater. 61 (1986) 48.
[28] M. Jagieła, Arch. Electr. Eng. 56 (2007) 57.
[29] A.J. Bergqvist, IEEE Trans. Magn. 32 (5) (1996) 4213.
[30] J.V. Leite, N. Sadowski, P. Kuo-Peng, N.J. Batistela, J.P.A. Bastos, A.A. de Espíndola, IEEE Trans. Magn. 40 (4) (2004) 1769–1775.
[31] P. Dimitropoulos, G.I. Stamoulis, E. Hristoforou, IEEE Sens. J. 6 (2006) 721.
[32] L. Bernard, L. Daniel, IEEE Trans. Magn. 51 (9) (2015) 7002513.
[33] A.P.S. Baghel, S.V. Kulkarni 043908-1, J. Appl. Phys 113 (2013).
[34] A.P.S. Baghel, K. Chwastek, S.V. Kulkarni, IET-Electr. Power Appl. 9 (2015) 344.
[35] A.P.S. Baghel, A. Gupta, K. Chwastek, S.V. Kulkarni, Physica-B 462 (2015) 86.
[36] C. Appino, M. Valsania, V. Basso, Physica-B 275 (2000) 103.
[37] M.F. de Campos, M.A. Campos, F.J.G. Landgraf, L.R. Padovese, J. Phys. 303 (2011) 012020.
[38] L. Néel, J. Phys. Radiat. 5 (1944) 241.
[39] M. Celasko, P. Mazzetti, IEEE Trans. Magn. 5 (1969) 372.
[40] G. Bertotti, Hysteresis in Magnetism, Academic Press, San Diego, 1998.
[41] M.F. de Campos, Proceedings of the XVIII IMEKO World Congress, Rio de Janeiro, Brazil, (2006).
[42] M. Emura, M.F. de Campos, F.L.G. Landgraf, J.C. Teixeira, J. Magn. Magn. Mater. 226 (2001) 1524.
[43] A.P.S. Baghel, S.K. Shekhawat, S.V. Kulkarni, I. Samajdar, Physica B 448 (2014) 349.
[44] A. Ramesh, D.C. Jiles, J.M. Roderick, IEEE Trans. Magn. 32 (1996) 4234.
[45] G.H. Shirkoohi, M.A.M. Aricat, IEEE Trans. Magn. 30 (1994) 928.
[46] R. Szewczyk, J. Mater. 7 (2014) 5109.
[47] D.C. Jiles, J.B. Thoelke, M.K. Devine, IEEE Trans. Magn. 28 (1992) 27.
[48] R.-A. Naghizadeh, B. Vahidi, S.H. Hosseinian, COMPEL 31 (2012) 1293.
[49] A.P.S. Baghel, S.V. Kulkarni, IET-Electr. Power Appl. 6 (2012) 689.
[50] T.R. Haller, J.J. Kramer, J. Appl. Phys. 41 (1970) 1034.
[51] K. Chwastek, J. Szczygłowski, W. Wilczyński, COMPEL 28 (2009) 603.
[52] A. Raghunatan, Y. Melikhov, J.E. Snyder, D.C. Jiles, J. Magn. Magn. Mater. 324 (2012) 20.
[53] K. Chwastek, A.P.S. Baghel, M.F. de Campos, S.V. Kulkarni, J. Szczygłowski, IEEE Trans. Magn. 51 (2015) 6000905.
[54] O. Perevertov, R. Schäfer 135001-135001, J. Appl. 45 (2012).
[55] O. Perevertov, R. Schäfer 185001-185001, J. Appl. 47 (2014).
[56] K.J. Rizzo, O. Hubert, L. Daniel, IEEE Trans. Magn. 46 (2010) 270.

Please cite this article as: A.P.S. Baghel, et al., Journal of Magnetism and Magnetic Materials (2016), http://dx.doi.org/10.1016/j.jmmm.2016.02.007